

pubs.acs.org/JPCB Article

# Interfacial Properties of Fluids Exhibiting Liquid Polyamorphism and Water-Like Anomalies

Published as part of The Journal of Physical Chemistry virtual special issue "Pablo G. Debenedetti Festschrift". Thomas J. Longo, Sergey V. Buldyrev, Mikhail A. Anisimov, and Frédéric Caupin\*



Cite This: J. Phys. Chem. B 2023, 127, 3079-3090



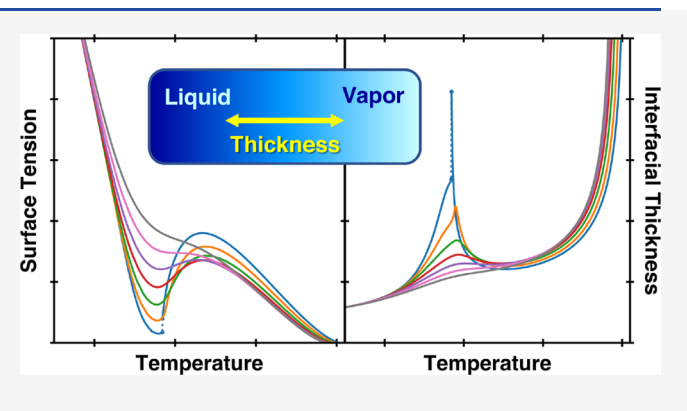
**ACCESS** I

III Metrics & More

Article Recommendations

s Supporting Information

ABSTRACT: It has been hypothesized that liquid polyamorphism, the existence of multiple amorphous states in a single-component substance, may be caused by molecular or supramolecular interconversion. A simple microscopic model [Caupin and Anisimov, *Phys. Rev. Lett.* 2021, 127, 185701] introduces interconversion in a compressible binary lattice to generate various thermodynamic scenarios for fluids that exhibit liquid polyamorphism and/or water-like anomalies. Using this model, we demonstrate the dramatic effects of interconversion on the interfacial properties. In particular, we find that the liquid—vapor surface tension exhibits either an inflection point or two extrema in its temperature dependence. Correspondingly, we observe anomalous behavior of the interfacial thickness and a significant



shift in the location of the concentration profile with respect to the location of the density profile.

#### 1. INTRODUCTION

Typically, pure substances may be found with only one gaseous or liquid state, while their solid state may exist in various polymorphic crystalline states. The existence of two distinct liquid forms in a single-component substance is more unusual, since liquids lack the long-range order common to crystals. However, the existence of multiple amorphous liquid states in a single-component substance, a phenomenon known as "liquid polyamorphism", <sup>1–4</sup> has been observed or predicted in a wide variety of substances, such as superfluid helium, <sup>5,6</sup> high-pressure hydrogen, <sup>7–11</sup> sulfur, <sup>12</sup> phosphorus, <sup>13,14</sup> carbon, <sup>15</sup> silicon, <sup>16–19</sup> silica, <sup>20,21</sup> selenium and tellurium, <sup>22,23</sup> and cerium. <sup>24</sup> Liquid polyamorphism is also highly plausible in deeply supercooled liquid water. <sup>1–4,25–33</sup>

In addition to the hypothesized existence of a liquid–liquid phase transition in supercooled water, other anomalies in water's thermodynamic properties have been reported, namely, a maximum in the temperature dependence of its isothermal compressibility<sup>34,35</sup> and a maximum in the isobaric heat capacity.<sup>36</sup> The possibility of anomalous behavior of the liquid–vapor surface tension,  $\sigma_{\rm LV}$ , of supercooled water has been a topic of long-standing interest. In 1951, an inflection point in the temperature dependence of  $\sigma_{\rm LV}$  was reported to occur near 0 °C,<sup>37</sup> but later studies, showing larger uncertainties, cast doubts on the early measurements.<sup>38,39</sup> Only recently, the highly accurate studies by Hrubý and coworkers became available.<sup>40–43</sup> Initially, in refs 40–42, it was concluded that no anomaly occurred in  $\sigma_{\rm LV}(T)$  down to

-26 °C; however, the results of the latest experiment, <sup>43</sup> reaching -31.4 °C, suggest that an inflection point might be possible. Theoretical studies support the existence of anomalies in liquid—vapor surface tension of supercooled water. <sup>44–50</sup> Using two closely related microscopic models of water-like associating fluids, Feeney and Debenedetti <sup>44</sup> predicted either an inflection point or a maximum, depending on the details and assumptions of the approach. Hrubý and Holten <sup>45</sup> proposed a two-state model able to generate an inflection point in the liquid—vapor surface tension of water. The inflection point has also been predicted by molecular dynamics simulations with several water potentials, such as SPC/E, <sup>46,47</sup> WAIL, <sup>48</sup> and TIP4P/2005. <sup>47,49,50</sup>

In the case of a fluid with a liquid—liquid phase transition, the liquid—liquid surface tension is also of particular interest. It controls the nucleation of the second liquid phase and the possibility of observing liquid—liquid coexistence in confined systems. For their models of water, Feeney and Debenedetti<sup>44</sup> found a liquid—liquid surface tension 2 orders of magnitude lower than the liquid—vapor one. They attributed

Received: December 20, 2022 Revised: March 9, 2023 Published: March 23, 2023





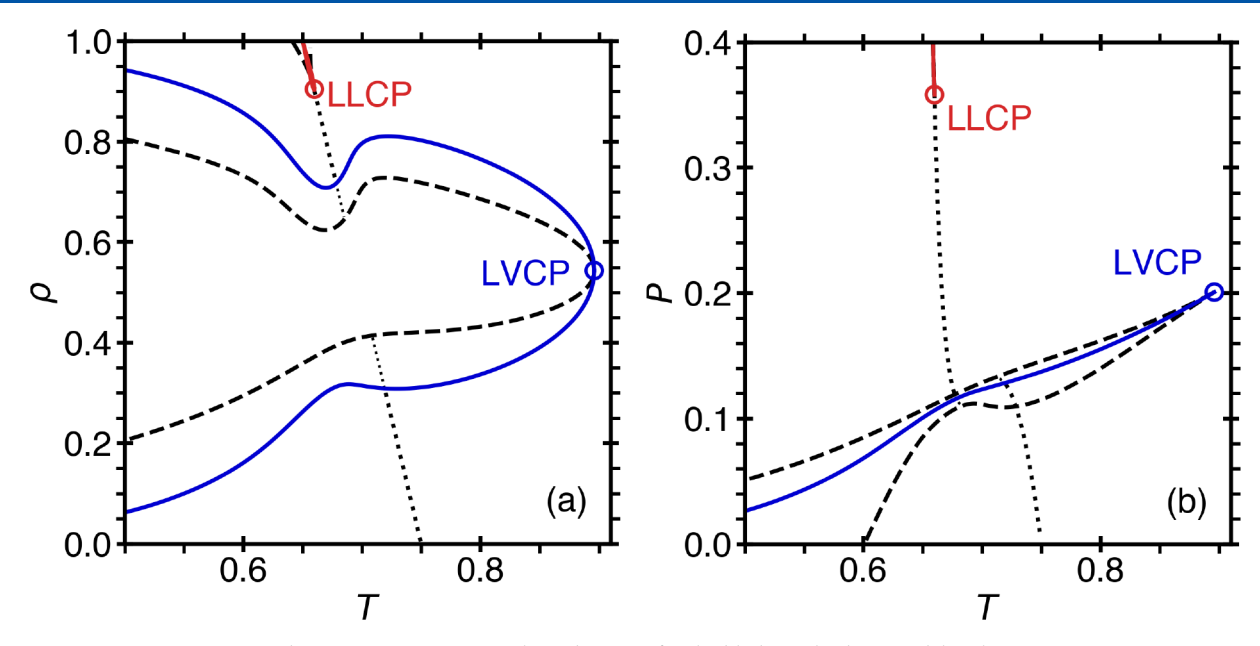


**Figure 1.** Density—temperature and pressure—temperature phase diagrams for the blinking-checkers model with  $\omega_{11} = 1.6$ ,  $\omega_{22} = 2.0$ ,  $\omega_{12} = 1.08$ ,  $\varepsilon = 3$ , and  $\varepsilon = 4$ . The liquid—vapor coexistence (blue curves) terminates at the liquid—vapor critical point, LVCP. The liquid—liquid coexistence (red curves) terminates at the liquid—liquid critical point, LLCP. The limits of thermodynamic stability (spinodals) are given by the dashed curves. The dotted line corresponds to the condition  $\varepsilon = 1/2$ , which qualitatively separates the regions enriched either by species 1 (at low temperatures and low densities) or species 2 (at high temperatures and high densities).

this phenomenon to the significant difference in the corresponding range of densities spanned by each transition.

In this work, inspired by the ideas of Feeney and Debenedetti, we investigate the interfacial properties in a simple microscopic model for liquid polyamorphism caused by the molecular interconversion between two species. Dur approach provides a first-principle derivation of the surface tension and the density and concentration interfacial profiles for the liquid—vapor interface, as well as for the corresponding liquid—liquid interfacial properties, if liquid polyamorphism takes place. We demonstrate that, depending on the interaction parameters between the two interconverting species, an inflection point or two extrema may emerge in the temperature dependence of the liquid—vapor surface tension.

#### 2. METHODS

In this section, we describe the model developed by Caupin and Anisimov,<sup>52</sup> referred to as the "blinking-checkers" lattice model, and its application in the density-gradient theory to calculate the interfacial properties.

**2.1. Blinking-Checkers Lattice Model.** We consider a compressible binary lattice of fixed total volume, V, where each of the N lattice sites can either be empty or occupied by one particle of two types (1 and 2). The numbers of particles of types 1 and 2 are  $N_1$  and  $N_2$ , respectively. The number density is  $\rho = (N_1 + N_2)/N$ , and the fraction of particles of type 1 in the mixture is  $x = N_1/(N_1 + N_2)$ . The interactions of each particle with its z nearest neighbors are given by interaction parameters between each particle type of the form  $\omega_{11} = -z\varepsilon_{11}/2$ ,  $\omega_{22} = -z\varepsilon_{22}/2$ , and  $\omega_{12} = -z\varepsilon_{12}/2$ , where the epsilons represent the energy of the pair interactions. There is no interaction with empty sites. The meanfield Helmholtz energy per lattice site, f = F/N, in the nonreacting version of the blinking-checkers model is given by

$$f(T, \rho, x) = \rho \varphi_2^{\circ} + \rho x \varphi_{12}^{\circ} - \rho^2 [\omega_{11} x^2 + \omega_{22} (1 - x)^2 + 2\omega_{12} x (1 - x)] + T[\rho x \ln x + \rho (1 - x) \ln(1 - x)] + T[\rho \ln \rho + (1 - \rho) \ln(1 - \rho)]$$
(1)

where  $\varphi_{12}^{\circ} = \varphi_{1}^{\circ} - \varphi_{2}^{\circ}$ , in which  $\varphi_{1}^{\circ} = \varphi_{1}^{\circ}(T)$  and  $\varphi_{2}^{\circ} = \varphi_{2}^{\circ}(T)$  are functions of temperature only, containing the arbitrary zero points of energy and entropy.<sup>3</sup> In eq 1, we adopt Boltzmann's constant,  $k_{\rm B}$ , as  $k_{\rm B} = 1$ . For the units of the various quantities in this work, see section S1 in the Supporting Information. The three terms in square brackets in eq 1 describe the contribution to the free energy from the energy of interactions, the entropy of mixing of the two species, and the entropy of mixing of the occupied and empty sites.

Since it has been hypothesized that the molecular interconversion of species could be a generic cause of liquid polyamorphism, 3,29,32 species 1 and 2 are allowed to interconvert via a simple reaction of the form,  $1 \rightleftharpoons 2$ . The blinking-checkers lattice is a generic model, which has been used to generate liquid polyamorphism and reproduce a variety of the anomalies in the thermodynamic properties of supercooled water.<sup>52</sup> Phenomenologically, species 1 and 2 could also represent supramolecular states 1 and 2, which enables one to use this model, via a coarse-grained approach, to mimic the different scenarios for the polyamorphic phase behavior considered for supercooled water. The most important aspect of mapping the blinking-checkers model to describe the phase behavior of polyamorphic substances is to assign the appropriate energy and entropy of reaction for the system.<sup>3,52</sup> Applying the condition for chemical-reaction equilibrium,  $\partial f/\partial x|_{T,\rho} = \mu_{12} = 0$ , where  $\mu_{12} = \mu_1 - \mu_2$  is the difference between the two chemical potentials of each species in the interconverting mixture, makes the temperaturedependent function,  $\varphi_{12}^{\circ}(T)$ , well-defined. We emphasize that, unlike previous models for water, which introduce a "local" density difference by changing the occupancy<sup>53</sup> or

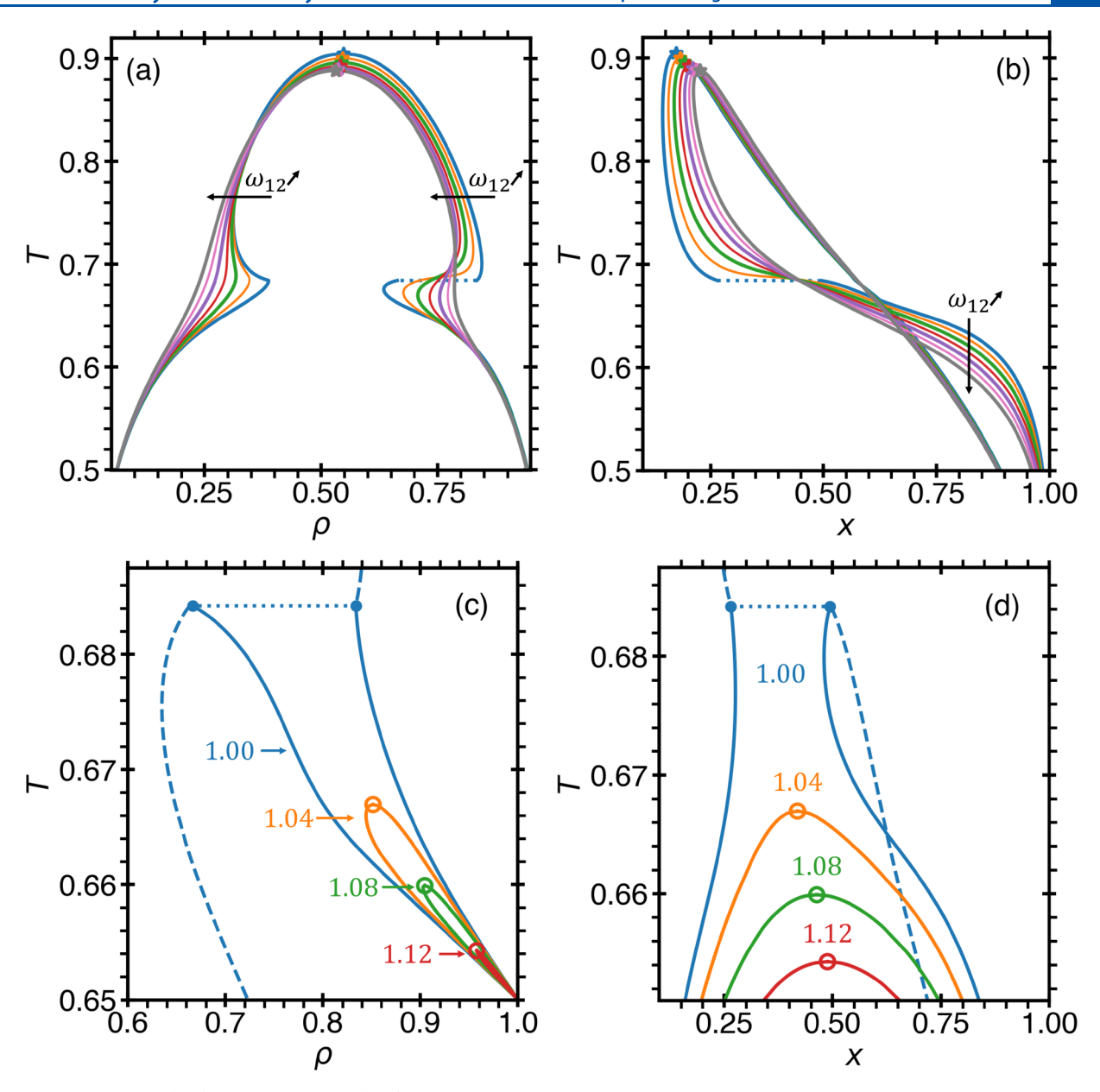


Figure 2. Liquid–vapor (a, b) and liquid–liquid (c, d) coexistence curves for the seven systems with  $ω_{11} = 1.6$ ,  $ω_{22} = 2.0$ , e = 3, and s = 4 and with various values of  $ω_{12}$ :  $ω_{12} = 1.00$  (blue),  $ω_{12} = 1.04$  (orange),  $ω_{12} = 1.08$  (green),  $ω_{12} = 1.12$  (red),  $ω_{12} = 1.16$  (purple),  $ω_{12} = 1.20$  (pink), and  $ω_{12} = 1.24$  (gray). The critical points, indicated by the stars in (a, b) and open circles in (c, d), are the unique liquid–vapor (LVCP) or liquid–liquid (LLCP) critical points in the interconverting system, referred to as "actual" critical points. In (a, b), the arrows indicate the direction of increasing  $ω_{12}$ . As also indicated in Figure 1, species 1 is enriched in the low-density, low-temperature region, while species 2 is enriched in the high-density, high-temperature region. For the system with  $ω_{12} = 1.00$ , in (c, d), the dashed blue curves indicate the liquid–vapor coexistence, while, in (a–d), the dotted line indicates the discontinuity at the triple point. For more details, see Supporting Information section S2.

volume <sup>54–57</sup> of each cell, the blinking-checkers model assumes that there is no volume change of reaction. This indicates that the nonideality of the mixture is the primary ingredient for the anomalous behavior of the thermodynamic properties in fluids exhibiting polyamorphic or water-like behavior. <sup>52</sup> We specify this function through the energy of reaction, e, and the entropy of reaction, s, as  $\varphi_{12}^0 = -(e-Ts)$ , the simplest linear approximation of this function. <sup>3,52</sup> The condition for chemical-reaction equilibrium,  $\mu_{12} = 0$ , reduces the number of thermodynamic degrees of freedom by one and defines the equilibrium concentrations (molecular fractions) of species 1,  $x = x_e(T, \rho)$ . Therefore, the concentration is no longer an independent variable, and thermodynamically, the intercon-

verting binary mixture thermodynamically behaves as a singlecomponent fluid.

Figure 1a and b illustrates the  $\rho$ -T and P-T phase diagram of the blinking-checkers lattice for an example set of interaction parameters ( $\omega_{11}=1.6$ ,  $\omega_{22}=2.0$ , and  $\omega_{12}=1.08$ ) and interconversion-reaction parameters (e=3 and s=4). For this choice of the energy and the entropy of reaction, we obtain a negative slope for the liquid-liquid phase transition, similar to that predicted for supercooled water. The line that qualitatively separates the region enriched by species 1, at low temperatures and low densities (referred to as "L1"), from the region enriched by species 2, at high temperatures and high densities (referred to as "L2"), is

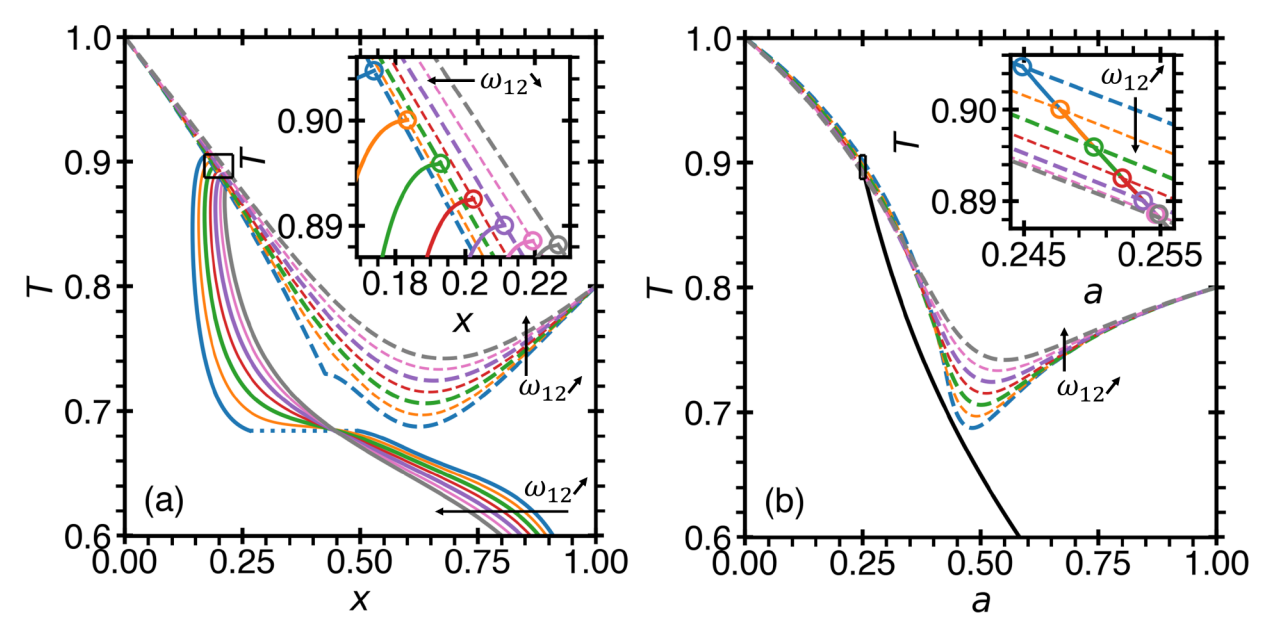


Figure 3. Illustration of the thermodynamic path selected by the interconversion reaction for e=3 and s=4 at constant volume, V, and at constant number of occupied lattice sites,  $N_1+N_2$ , represented through (a) the liquid branch of the liquid–vapor temperature–concentration coexistence (see Figure 2b) and (b) the activity,  $a=1/[1+e^{-\Delta\mu_{12}/k_BT}]$ , for the systems with different interaction parameters:  $\omega_{12}=1.00$  (blue),  $\omega_{12}=1.04$  (orange),  $\omega_{12}=1.08$  (green),  $\omega_{12}=1.12$  (red),  $\omega_{12}=1.16$  (purple),  $\omega_{12}=1.20$  (pink), and  $\omega_{12}=1.24$  (gray). For each system, the liquid–vapor critical line (LVCL) is shown by the dashed curves, while the collapsed coexistence, in (b), is illustrated by the black curve. The insets show the LV critical points for each scenario. In (a, b), the black arrow indicates the direction of increasing (or decreasing)  $\omega_{12}$ . Note that, for the system with  $\omega_{12}=1.00$ , the thermodynamic path crosses through the triple point, indicated by the dotted line in (a). For more details, see ref 52 and Supporting Information section S2.

indicated by the dotted line in Figure 1a,b. Furthermore, for this set of interaction parameters, two critical points and a "bottleneck" in the liquid–vapor coexistence are observed. The  $\rho$ –T and x–T phase diagrams for seven systems are illustrated in Figure 2a,b; see more details in Supporting Information sections S1 and S2. We note that, for different sets of parameters, one may obtain multiple fluid–fluid critical points, representing the more complex phase behavior of polyamorphic fluids.

In the treatment of the blinking-checkers model, we utilize the meanfield approximation, which is more accurate in the region away from the critical point, where the correlation length of concentration or density fluctuations is not significantly larger than the distance between molecules (the Ginzburg criterion<sup>58</sup>). To estimate the effect of the critical fluctuations on the phase behavior, we also conducted exact Monte Carlo (MC) simulations of the blinking-checkers model. The preliminary results of these simulations, presented in Supporting Information sections S3 and S12, demonstrate a qualitatively similar bottleneck anomaly of the liquid-vapor coexistence as well as interfacial profile behavior near the minimum of this bottleneck. Also, these simulations have confirmed that the phase transitions in the interconverting blinking-checkers model belong to the three-dimensional Isingmodel universality class.59

**2.2. Virtual Critical Points.** If interconversion does not occur, the blinking-checkers model describes a compressible binary mixture, which may exhibit liquid–vapor and liquid–liquid coexistence, as well as the corresponding critical lines.<sup>52</sup> Consider a point on a critical line with temperature,  $T_{co}$  density,  $\rho_{co}$  and type 1 particles' molecular fraction,  $x_{co}$ . In a fixed volume, V, the corresponding critical isochore, at fixed composition, contains a fixed number of particles 1 and 2,

given by  $\rho_c x_c V$  and  $\rho_c (1-x_c) V$ , respectively. At temperatures below  $T_c$ , the system will separate in two phases,  $\alpha$  and  $\beta$  (which could be liquid and vapor or liquid and liquid). For phase  $i=\alpha$  or  $\beta$ , let  $\rho_i$ ,  $x_i$ , and  $V_i$  be the density, type 1 fraction, and volume, respectively. At each  $T \leq T_c$ , the six values  $(\rho_i, x_i, V_i)_{i=\alpha,\beta}$  are fully determined by three conservation equations (one for volume and two for mass) and three equilibrium conditions (two for the chemical potentials and one for the pressure).

As explained in the previous section, when interconversion takes place, the system (in terms of the Gibbs phase rule<sup>58</sup>) thermodynamically behaves as a single-component fluid, following the given paths along liquid-vapor or liquid-liquid coexistence in the two-phase region. Therefore, for each point along the interconversion path, there is a corresponding critical point of the nonreacting binary mixture, which is connected to this point on the path by a critical isochore for the nonreacting mixture at fixed composition. We refer to this corresponding binary-mixture critical point as the "virtual" (i.e., invisible along the interconversion path) critical point, while we refer to the interconverting system's unique liquid-vapor critical point (LVCP) as the "actual" LVCP. Similarly, for systems exhibiting interconversion, we refer to the single liquid-liquid critical point (LLCP) as the actual LLCP. We emphasize that not only the phase diagram of the interconverting mixture is characterized by unique fluid-fluid critical points (like that of a single-component fluid), but the response functions, second derivatives of the free energy at  $\mu_{12} = 0$ , also exhibit the singularities characteristic of single-component fluids.

An illustration of the thermodynamic path along liquid–vapor equilibrium in the interconverting fluid for seven different sets of interaction parameters,  $\omega_{12}$ , is shown in Figure 3a. In the coexisting liquid and vapor phases, there are

two branches of the density and concentration, given by  $\rho_{\rm L}^{\rm cxc}(T)$ ,  $\rho_{\rm V}^{\rm cxc}(T)$ ,  $x_{\rm L}^{\rm cxc}(T)$ , and  $x_{\rm V}^{\rm cxc}(T)$ ; see Figure 2a,b for details. For simplicity, in Figure 3a, we show only the liquid branch of the liquid–vapor coexistence; see Figure 2b for both branches. The liquid–vapor critical lines for the seven binary mixtures with the same interaction parameters are also shown (dashed lines). Figure 3b displays the same, but the abscissa, x, is replaced by the "activity",  $a = 1/[1 + {\rm e}^{-\Delta\mu_{12}/k_{\rm B}T}],^{60-62}$  where  $\Delta\mu_{12} = \mu_{12} - \varphi_{12}^0$ ; see Supporting Information section S1 for details. Since, due to the chemical reaction equilibrium condition,  $\mu_{12} = 0$  and  $\varphi_{12}^{\rm o} = -(e - Ts)$ ,  $\Delta\mu_{12}$  is given by

$$\Delta \mu_{12} = -\varphi_{12}^{\circ} = e - Ts \tag{2}$$

(see Supporting Information section S1 for details). Thus, for each point along the thermodynamic path selected by interconversion, the activity is restricted by eq 2, such that, for the seven systems considered in this work, the activities collapse into the line shown in Figure 3b, as only  $\omega_{12}$  is varied in each system.

The proximity of the virtual critical line affects the properties along coexistence in the interconverting fluid, causing, in particular, the bottlenecked shape of the  $\rho$ -T liquid-vapor coexistence (Figure 2). For our selection of the interaction parameters, this particular effect is pronounced because the difference between  $\omega_{11}$  and  $\omega_{22}$  is significant ( $\omega_{11}$  = 1.6 and  $\omega_{22}$  = 2.0). In addition, the asymmetry of the liquid-vapor coexistence occurs due to the existence of the liquid-liquid critical point, and even occurs in the singularity-free scenario where the liquid-liquid critical point is moving to indefinite pressure (see ref 52 and Supporting Information section S2 for more details).

**2.3.** Interfacial Properties via Density Gradient Theory. To model the fluid interfaces, we consider density gradient theory (DGT), 63-67 in which the free energy of the system is expanded in a Taylor series up to second-order in terms of derivatives of the concentration and density with respect to the coordinate perpendicular to the interface. Following the ideas presented by van der Waals, 68,69 and later elaborated by Cahn and Hilliard, the interfacial tension of a binary fluid may be expressed as 66,71,72

$$\sigma = \int \left[ \Delta \Omega(x, \rho, T) + \frac{1}{2} c_x(\rho) |\nabla x|^2 + \frac{1}{2} c_\rho(x) |\nabla \rho|^2 + c_{\rho, x}(\rho, x) |\nabla \rho|^2 \right] dV$$
(3)

where  $c_x$ ,  $c_\rho$ , and  $c_{\rho,x}$  are the microscopic "influence" coefficients.  $\Delta\Omega$  is the excess grand potential per lattice site, given by  $^{66}$ 

$$\Delta\Omega(x, \rho, T) = f(x, \rho, T) - \rho x \mu_2^{\text{cxc}} - \rho (1 - x) \mu_1^{\text{cxc}} + P^{\text{cxc}}$$
(4)

where  $\mu_1$ ,  $\mu_2$  and P are the chemical potentials of species 1 and 2 per lattice site in solution and the pressure per lattice site, respectively, while the superscript "cxc" indicates that the quantity is evaluated along the phase coexistence. We note that  $\Delta\Omega$  may be calculated for a nonreactive mixture, as in eq 4, or it may be calculated for a reactive mixture. Importantly, in either case, due to the chemical-reaction equilibrium condition, the grand thermodynamic potential is the same for the nonreacting and for the reacting cases of the blinking-checkers model (see Supporting Information section S5 for details).

Assuming planar fluid interfaces in the lattice, we find that the three influence coefficients for the concentration and density are related to the interaction parameters by

$$c_{x}(\rho) = \frac{1}{2}l^{2}\rho^{2}\omega \tag{5}$$

$$c_{\rho}(x) = \frac{1}{2}l^{2}[\omega_{11}x^{2} + 2\omega_{12}x(1-x) + \omega_{22}(1-x)^{2}]$$
 (6)

$$c_{\rho,x}(\rho, x) = \frac{1}{2} l^2 \rho [\omega_{11} x + \omega_{12} (1 - 2x) - \omega_{22} (1 - x)]$$
(7)

where  $\omega = \omega_{11} + \omega_{22} - 2\omega_{12}$  and l is the length of a lattice cell (see Supporting Information section S6 for the full derivation). Note that, in the language of ref 44, eqs 5–7 define the influence coefficients *a priori* with the assumption that the gradients contribute to the local energy density but not to the entropy density.

To determine the interfacial profiles, we adopt a variational approach, based on a family of anzatz functions, choosing the optimal one by minimizing the interfacial tension, given by eq 3. We have also obtained exact numerical solutions for the profiles by solving the equilibrium condition for the surface tension, which is obtained from eq 3, 66,71,72

$$\Delta\Omega(x, \rho, T) = \frac{1}{2}c_x(\rho)|\nabla x|^2 + \frac{1}{2}c_\rho(x)|\nabla \rho|^2 + c_{\rho,x}(\rho, x)\nabla\rho\cdot\nabla x$$
(8)

as explained in section S6 in the Supporting Information. We find that the variational approach is enough to capture the anomalous behavior of the interfacial properties with sufficient accuracy (see Supporting Information section S6 for details). Throughout the main text, we report the variational results, based on the Fisher–Wortis profile, which accounts for the thermodynamic asymmetry between the two coexisting phases. A comparison with an alternative symmetric ansatz is also discussed in Supporting Information section S6. The Fisher–Wortis ansatz is given in normalized form as a combination of symmetric and asymmetric components for both the density and concentration (molecular fraction) profiles as

$$\hat{\rho}(\hat{z}) = \frac{\rho(\hat{z}) - \rho_{\alpha}}{\rho_{\beta} - \rho_{\alpha}} = \hat{\rho}_{\text{sym}}(\hat{z}) + \Delta \hat{\rho}_{\text{d}} \hat{\rho}_{\text{asym}}(\hat{z})$$
(9)

$$\hat{x}(\hat{z}) = \frac{x(\hat{z}) - x_{\alpha}}{x_{\beta} - x_{\alpha}} = \hat{x}_{\text{sym}}(\hat{z}) + \Delta \hat{x}_{\text{d}} \hat{x}_{\text{asym}}(\hat{z})$$
(10)

where the symmetric contributions to the profiles are given by

$$\hat{\rho}_{\text{sym}}(\hat{z}) = \frac{1}{2} \left[ \tanh \left( \frac{\hat{z}}{\hat{\xi}} \right) + 1 \right]$$
(11)

$$\hat{x}_{\text{sym}}(\hat{z}) = \frac{1}{2} \left[ \tanh \left( \frac{\hat{z} + \hat{\delta}}{\hat{\zeta}} \right) + 1 \right]$$
(12)

and where the asymmetric contributions to the profiles are given by

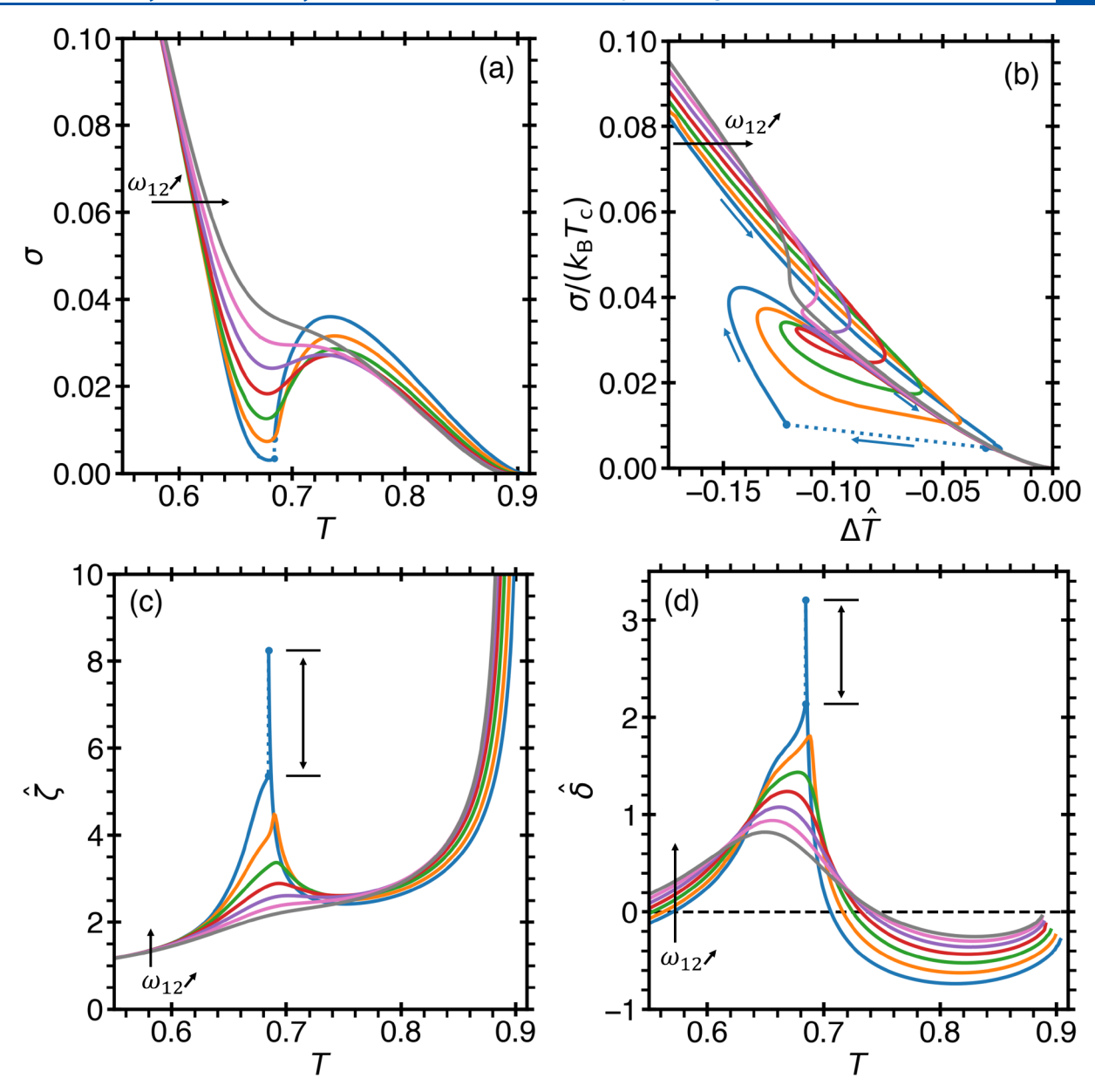


Figure 4. Liquid—vapor interfacial tension as a function of temperature (a), and also presented in reduced units (b), for the system with  $\omega_{12}=1.00$  (blue),  $\omega_{12}=1.04$  (orange),  $\omega_{12}=1.08$  (green),  $\omega_{12}=1.12$  (red),  $\omega_{12}=1.16$  (purple),  $\omega_{12}=1.20$  (pink), and  $\omega_{12}=1.24$  (gray). In (b), the critical temperature is given by the "virtual" critical point (for the nonreactive binary mixture) for each concentration along the thermodynamic path selected by the interconversion reaction. The blue arrows indicate the direction of warming. (c) The reduced interfacial thickness,  $\hat{\zeta}=\zeta/l$ , and (d) the reduced relative distance between the concentration and density profiles,  $\hat{\delta}=\delta/l$ . In (a–d), the black arrow indicates the direction of increasing  $\omega_{12}$ , and the dotted lines indicate the discontinuity of the interfacial properties for the system with  $\omega_{12}=1.00$  at the triple point, shown by the vertical bars in (c, d).

$$\hat{\rho}_{\text{asym}}(\hat{z}) = \tanh^2 \left(\frac{\hat{z}}{\hat{\zeta}}\right) + \frac{\ln\left[\cosh\left(\frac{\hat{z}}{\hat{\zeta}}\right)\right]}{\cosh^2\left(\frac{\hat{z}}{\hat{\zeta}}\right)} - (\rho_{\beta} - \rho_{\alpha})$$
(13)

$$\hat{x}_{\text{asym}}(\hat{z}) = \tanh^2 \left( \frac{\hat{z} + \hat{\delta}}{\hat{\zeta}} \right) + \frac{\ln \left[ \cosh \left( \frac{\hat{z} + \hat{\delta}}{\hat{\zeta}} \right) \right]}{\cosh^2 \left( \frac{\hat{z} + \hat{\delta}}{\hat{\zeta}} \right)} - (x_{\beta} - x_{\alpha})$$
(14)

in which  $\hat{z}=z/l$  is the normalized coordinate perpendicular to the planar interface, the subscripts " $\alpha$ " and " $\beta$ " indicate the

coexisting phases,  $\hat{\zeta} = \zeta/l$  is the normalized interfacial thickness, and  $\hat{\delta} = \delta/l$  is the normalized shift between the concentration and density profiles. The coefficient of the asymmetric terms in eqs 9 and 10 is the reduced diameter for the density and concentration, given by

$$\Delta \hat{\rho}_{\rm d} = \frac{\rho_{\beta} + \rho_{\alpha}}{2\rho_{\rm c}} - 1 \tag{15}$$

$$\Delta \hat{x}_{\rm d} = \frac{x_{\beta} + x_{\alpha}}{2x_{\rm c}} - 1 \tag{16}$$

where  $\rho_c$  and  $x_c$  are the critical points determined from the nonreacting blinking-checkers model, referred to as virtual critical points; see section 2.2. The diameters with respect to the virtual critical points are provided in Supporting Information section S7 for each system investigated. Relative to the liquid–vapor coexistence, for the liquid–liquid coexistence, the diameters are small, such that the asymmetric contribution to the liquid–liquid interfacial profiles is also minimal

Due to the lack of a theory to account for the interfacial profile asymmetry in compressible binary fluids, we choose the Fisher–Wortis ansatz, even though it was originally developed for a single-component substance. This ansatz contains only two free parameters,  $\hat{\zeta}$  and  $\hat{\delta}$ , less than the symmetric ansatz, and it partially reproduces the asymmetry of the exact solution (see details in Supporting Information section S6).

#### 3. RESULTS AND DISCUSSION

In this section, we demonstrate the anomalous behavior of the interfacial properties in the blinking-checkers lattice model. We also discuss the conditions for observing either an inflection point or extrema in the liquid—vapor interfacial tensions.

3.1. Liquid-Vapor Interfacial Tensions. Using the Fisher-Wortis ansatz, the liquid-vapor interfacial tension along the thermodynamic path (selected by interconversion) as a function of temperature is presented in Figure 4a for seven systems. We find that all scenarios exhibit either an inflection point or two extrema. Of the two scenarios that exhibited an inflection point but not extrema ( $\omega_{12} = 1.20$  and  $\omega_{12} = 1.24$ ), both were "singularity free scenarios" (exhibiting no liquidliquid phase transition)52 whose thermodynamic path was relatively far away from the liquid-vapor critical line; see Figure 3. Each of the remaining scenarios exhibit a maximum and minimum depending on the proximity of the selected thermodynamic path to the liquid-vapor critical line, including the singularity-free system with  $\omega_{12}$  = 1.16 [During the review of the present work, we became aware of a recent phenomenological density functional study of another waterlike model<sup>75</sup> also reporting two extrema in the temperature dependence of the liquid-vapor interfacial tension]. The scenarios for which the liquid-vapor coexistence was interrupted by the triple point ( $\omega_{12} = 1.00$ ) exhibit a discontinuity of the liquid-vapor surface tension at this point.

The reduced interfacial tension, expressed through the distance to the virtual LV critical temperature  $\Delta \hat{T} = 1 - T/[T_{\rm c}(x)]$ , is illustrated in Figure 4b. Systems exhibiting two extrema in their interfacial tension demonstrate a "looping" pattern as the thermodynamic path approaches and then deviates from the virtual LVCL. As the interconverting systems approach their actual LV critical points, the surface tension asymptotically follows the meanfield power law  $\sigma \sim |\Delta \hat{T}|^{3/2}$  (see Supporting Information section S9 for details).

In the region where the surface tension reaches a minimum, the interfacial thickness, presented in Figure 4c, correspondingly reaches a maximum. This phenomenon occurs since the thermodynamic path approaches the virtual LVCL. A DGT treatment of the liquid-vapor interface of real water<sup>76</sup> reported the possibility of a minimum in the temperature dependence of the interfacial thickness (as observed in several cases here), depending on the equation of state used to describe metastable water. We also note that, in particular, for

the system with  $\omega_{12}$  = 1.00, the interfacial thickness exhibits a discontinuity at the triple point temperature (see Table 1). We

Table 1. Surface Tension  $\sigma$ , Normalized Interfacial Thickness  $\hat{\zeta}=\zeta/l$ , and Normalized Shift  $\hat{\delta}=\delta/l$  for the Three Coexisting Phases (Liquid 1, Liquid 2, and Vapor) for the System with  $\omega_{12}=1.00$  at the Triple Point Temperature (T=0.6843)

	$\sigma$	ξ	$\hat{\delta}$
L1-V	0.00793	8.242	3.203
L2-V	0.00334	5.372	2.145
L1-L2	0.00321	6.040	0.983

also estimate that the DGT approximation breaks down when the interface becomes sharp. We estimate that a sharp liquidvapor interface has an interfacial tension of  $\sigma_{\rm shp} \approx \omega_{11}/8 = 0.2$ , which is reached around T = 0.5, where the interfacial thickness becomes comparable to the size of the lattice cell,  $\hat{\zeta} = 1$  (see Supporting Information section S10 for details). For each system in the vicinity of the liquid-vapor critical point, we found that the interfacial thickness followed an asymptotic power law of the from  $\hat{\zeta} \sim |\Delta \hat{T}|^{-0.38}$ , which deviates from the van der Waals meanfield asymptotic power law, <sup>69</sup>  $\hat{\zeta} \sim |\Delta \hat{T}|^{-0.5}$ , for the thickness of the order-parameter interface (see Supporting Information section S9 for details). As predicted by the complete scaling theory, 77-79 the order parameter for the compressible binary mixture is a nonlinear combination of  $\rho$  and  $\alpha$ . Thus, the discrepancy in the asymptotic behavior of the interfacial thickness may be attributed to the assumption that the thickness for the density and concentration profiles is the same as that for the order parameter in the Fisher-Wortis ansatz; see eqs 9 and 10.

The inflection points of the concentration and density profiles are related through the shift  $\delta$ , which was included in the concentration profile ansatz, eq 10. In the first-order approximation,  $\delta$  can be separated into symmetric and asymmetric contributions as  $\delta = \delta_{\text{sym}} + \delta_{\text{asym}}$ . The symmetric contribution is proportional to the difference in the centers of each profile,  $\delta_{\text{sym}} \sim x[\hat{z}=0] - \rho[\hat{z}=0]$ , while the asymmetric contribution is proportional to the difference in diameters,  $\delta \sim \Delta \hat{x}_{\rm d} - \Delta \hat{\rho}_{\rm d}$  (see Supporting Information section S11 for details). The effects of asymmetry on near-critical interfacial profiles in the scaling theory of inhomogeneous fluids were considered in ref 80. In the region of the anomalous behavior of the surface tension, this shift reaches a maximum as illustrated in Figure 4d. Similarly to the interfacial thickness, the shift is also discontinuous at the triple point temperature (see Table 1). Meanwhile, at the actual LV critical temperature,  $\delta$  approaches a finite value, while both the density and concentration profiles exhibit a diverging thickness and a vanishing amplitude. Simultaneously, at this temperature, the numerical calculation becomes uncertain due to the large fluctuations of density and concentration (see Supporting Information section S8 for details).

**3.2. Liquid**—**Liquid Interfacial Tensions.** The liquid—liquid interfacial tensions were calculated for the four systems exhibiting liquid polyamorphism ( $\omega_{12} = 1.00$ ,  $\omega_{12} = 1.04$ ,  $\omega_{12} = 1.08$ , and  $\omega_{12} = 1.12$ ) with use of the Fisher—Wortis ansatzes for the density and concentration profiles, eqs 9 and 10, and are illustrated in comparison with the liquid—vapor interfacial

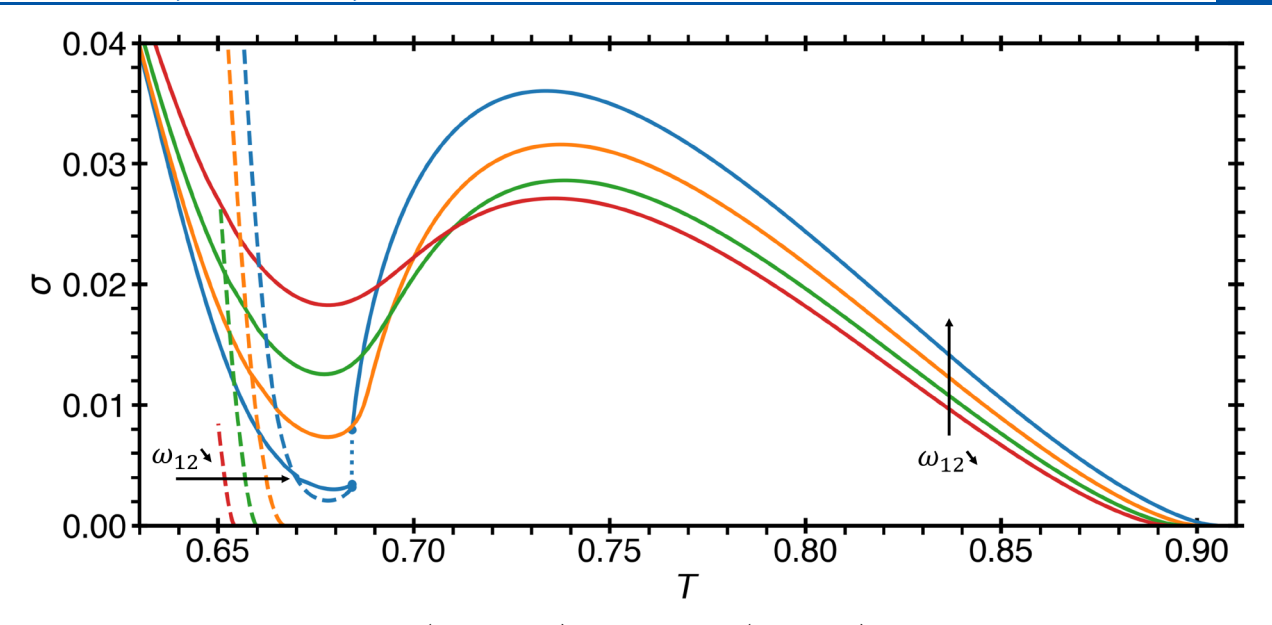


Figure 5. Comparison between the liquid–liquid (dashed curves) and liquid–vapor (solid curves) interfacial tensions as a function of temperature for the system with  $\omega_{12}=1.00$  (blue),  $\omega_{12}=1.04$  (orange),  $\omega_{12}=1.08$  (green), and  $\omega_{12}=1.12$  (red). The dotted blue line indicates the discontinuity in the liquid–vapor interfacial tension, while the black arrows indicate the direction in which  $\omega_{12}$  is decreasing.

tension in Figure 5 (more details in Supporting Information section S8). We find that, for three systems ( $\omega_{12}=1.00$ ,  $\omega_{12}=1.04$ , and  $\omega_{12}=1.08$ ), the liquid—liquid interfacial tension crosses that of the liquid—vapor, being larger for lower temperatures. <sup>44</sup> This is different from the conclusion of Feeney and Debenedetti <sup>44</sup> that  $\sigma_{\rm LL}$  is fundamentally lower than  $\sigma_{\rm LV}$  at the same temperature. Indeed, this behavior is observed when the bottleneck in the liquid—vapor coexistence is absent, as in the case of ref 44, or not very deep, as in our model for the system with  $\omega_{12}=1.12$ . Depending on the choice of parameters in the blinking-checkers model,  $\sigma_{\rm LL}$  may be large away from the LLCP; however, as the LLCP is approached, the ratio  $\sigma_{\rm LL}/\sigma_{\rm LV}$  must vanish.

We note that, for the liquid-liquid interfacial tension, the DGT is a good approximation everywhere as the liquid-liquid coexistence approaches infinite pressures before forming a sharp interface between the two liquid phases. We estimate that a sharp interface forms where  $\sigma_{\rm shp} \approx \omega/8$  , which goes from  $\sigma_{\rm shp} pprox$  0.2 for the system with  $\omega_{12}$  = 1.00 to  $\sigma_{\rm shp} pprox$  0.17 for the system with  $\omega_{12}$  = 1.12, which is larger than any of the liquid liquid interfacial tensions observed in the model (see details in Supporting Information section S10). For the system with  $\omega_{12}$ = 1.00, the liquid-liquid interfacial tension is smaller than both the liquid 1-vapor or the liquid 2-vapor interfacial tensions (see Table 1 for details). The reduced interfacial thicknesses,  $\hat{\zeta}$ , and the reduced shifts between the concentration and density profiles,  $\hat{\delta}$ , are provided in Supporting Information section S8. In particular, we note that, for the systems that reach a liquid-liquid critical point ( $\omega_{12} = 1.04$ ,  $\omega_{12}$  = 1.08, and  $\omega_{12}$  = 1.12), the liquid-liquid interfacial tension does not demonstrate any anomalous behavior. Furthermore, the interfacial tensions and interfacial thicknesses follow the predicted meanfield asymptotic power laws (see Supporting Information section S9 for details). Moreover, in the system with  $\omega_{12}$  = 1.00, the liquid-liquid interfacial tension exhibits a minimum prior to the triple point temperature.

**3.3. Interfacial Profiles.** We now investigate the interfacial profiles for density and concentration. Parts a and b of Figure 6 show the interfacial profiles predicted from the Fisher–Wortis ansatzes, eqs 9 and 10, for the system with  $\omega_{12} = 1.08$  at the temperatures that correspond to the maximum and minimum of the LV interfacial tension. We find that, at the minimum, the interfacial profiles are relatively symmetric, while, at the maximum, the concentration profile contains a large asymmetric contribution. The large asymmetry predicted by the Fisher–Wortis concentration ansatz occurs since the diameter of the concentration,  $\Delta \hat{x}_d$ , reaches a maximum at this temperature (see more details in Supporting Information section S7).

For the system with  $\omega_{12}$  = 1.00, at the triple point temperature,  $T_{\rm TP}$  = 0.6843, all of the interfacial properties exhibit a discontinuity (see Table 1). Since the interfacial tension of the L1-V (low-density-liquid-vapor) interface is much larger than the other two interfacial tensions, then, in accordance with Antonov's rule,  $\sigma_{L1,L2} < \sigma_{L1,L2}$ predict that the L1-V interface will be enriched (wetted) by the L2 (high-density-liquid) phase to reduce the energetically unfavorable L1-V interface. This indicates that the nonmonotonic behavior of the liquid-vapor interfacial tension may be caused by the surface enrichment of the L2-V coexistence by species 1. This behavior was confirmed by the interfacial profiles obtained in MC simulations of the blinkingcheckers model near the minimum of the interfacial tension (see Supporting Information section S12 for details). Notwithstanding this complete wetting phenomenon, we display in Figure 6c and d the interfacial profiles for the density and concentration of the three coexisting phases at the triple point.

**3.4.** Conditions for Anomalous Interfacial Behavior. We note that, based on the findings presented in this work, no general conclusion about the absence of a liquid—liquid transition can be drawn from the existence of an inflection point in the liquid—vapor interfacial tension. For instance, on one hand, in the present work, the inflection point is observed only for singularity free scenarios; on the other hand, the

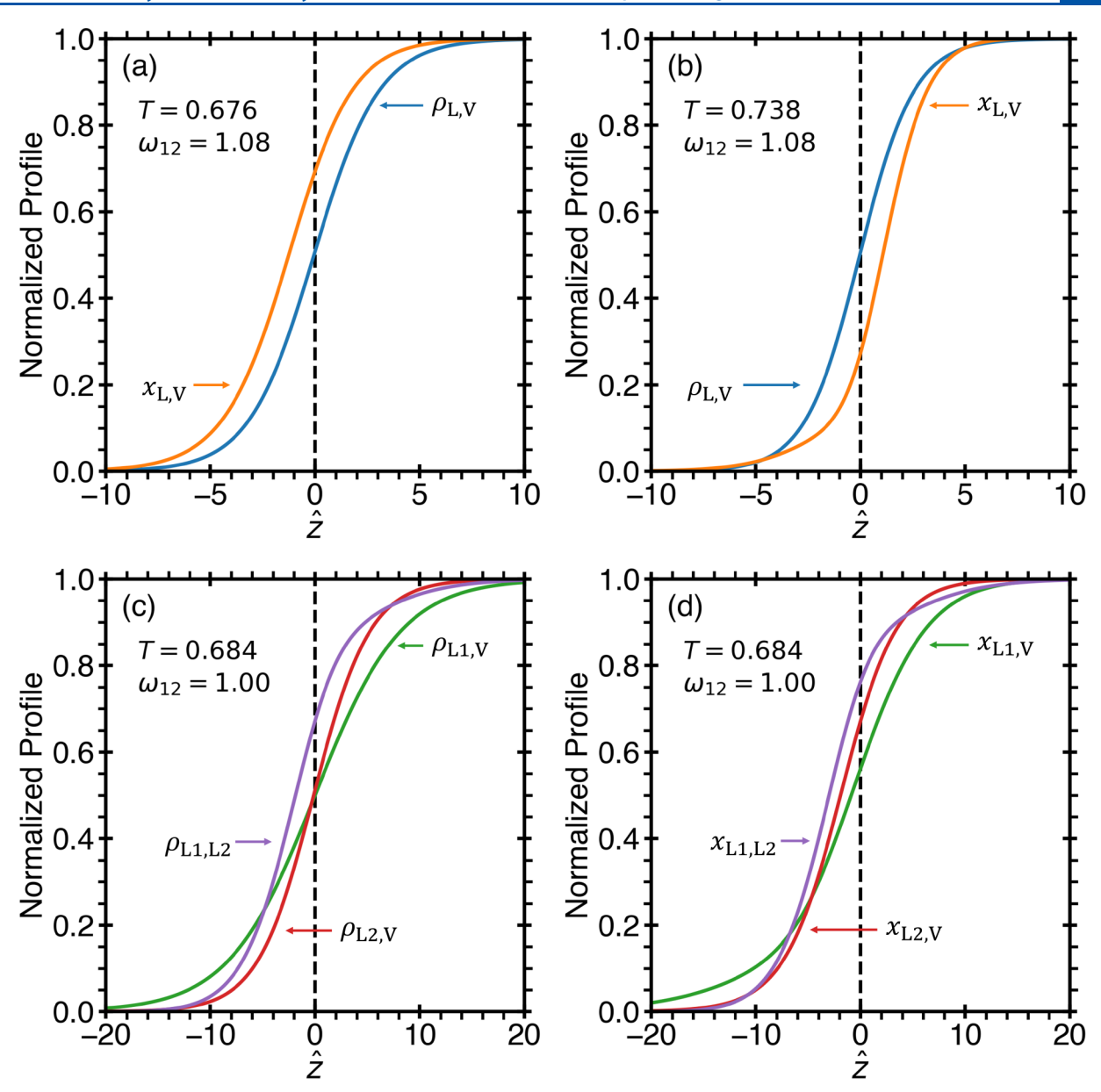


**Figure 6.** Normalized density and concentration liquid—vapor profiles as a function of the coordinate perpendicular to the planar interface,  $\hat{z}=z/l$ , given by eqs 9 and 10 for the system with  $\omega_{11}=1.6$ ,  $\omega_{22}=2.0$ ,  $\omega_{12}=1.08$ , e=3, and s=4 at the two temperatures (a, b) that correspond to the two extrema of the liquid—vapor interfacial tension (shown in Figure 4). Normalized (c) density and (d) concentration profiles for three-phase coexistence at the triple point,  $T_{\rm TP}=0.6843$ , for the system with  $\omega_{11}=1.6$ ,  $\omega_{22}=2.0$ , and  $\omega_{12}=1.00$ .

TIP4P/2005 model of water exhibits an inflection point, 47,49,50 while it is thought to possess a liquid-liquid transition terminated by a critical point. 31,81,82 We emphasize that the anomaly in the temperature dependence of the interfacial tension is linked to the anomaly in the liquid-vapor coexistence along the thermodynamic path selected by interconversion, and originates in the region where the equilibrium fraction of species,  $x_e$ , most dramatically changes, a concept that was first suggested by Hrubý and Holten.<sup>45</sup> It follows from our results that the shape of the LV coexistence is affected by two factors: the proximity to the virtual LVCL and the existence of the liquid-liquid phase transition. We note that this result is elucidated through the simplicity of the blinking-checkers lattice model, and may be observed in more complex (microscopic) models of fluids exhibiting polyamorphism and water-like anomalies. For instance, the

anomalies in supercooled water can be interpreted as the results of the interconversion of two supramolecular structures. This interconversion occurs only at low temperatures, extremely far away from the liquid—vapor critical point. Thus, there is a density maximum (at 4 °C) and a minimum (cutoff by the limit of spontaneous ice formation) only in the liquid branch of the LV coexistence in water. Onsequently, the LV surface tension may exhibit a maximum or an inflection point depending on the depth of the minimum.

#### 4. CONCLUSION

We investigated the interfacial properties of fluids exhibiting liquid polyamorphism and/or water-like anomalies modeled through a compressible binary lattice with molecular interconversion of species. We demonstrated that the change in the equilibrium fraction of the interconverting species as a

function of temperature is the origin of various thermodynamic anomalies, e.g., in density and in surface tension. We found that, due to the proximity of the thermodynamic path, selected by the interconversion of species, to the liquid-vapor critical line of the nonreacting binary mixture, the liquid-vapor interfacial tension demonstrates an anomalous temperature dependence, exhibiting either two extrema or an inflection point. In the anomalous region, where the liquid-vapor interfacial tension exhibits a minimum, the interfacial thickness and the relative distance between the density and concentration interfacial profiles exhibit a maximum. Moreover, in the scenario where the fluid possesses a triple point between the three coexisting fluid phases, we predict a discontinuity in the interfacial properties as well as complete wetting of the lowdensity-liquid and vapor interface by the high-density-liquid phase.

## ASSOCIATED CONTENT

#### Supporting Information

The Supporting Information is available free of charge at https://pubs.acs.org/doi/10.1021/acs.jpcb.2c08901.

Further description and calculations of the blinking-checkers model, a comparison of the exact solution of the interfacial properties with phenomenological asymmetric ansatzes, and results of Monte Carlo simulations (PDF)

#### AUTHOR INFORMATION

#### **Corresponding Author**

Frédéric Caupin — Institut Lumière Matière, Université de Lyon, Université Claude Bernard Lyon 1, CNRS, Institut universitaire de France, F-69622 Villeurbanne, France; orcid.org/0000-0002-8892-2514;

Email: frederic.caupin@univ-lyon1.fr

### Authors

Thomas J. Longo — Institute for Physical Science and Technology, University of Maryland, College Park, Maryland 20742, United States; Occid.org/0000-0002-2423-7788

Sergey V. Buldyrev – Department of Physics, Yeshiva University, New York, New York 10033, United States; Department of Physics, Boston University, Boston, Massachusetts 02215, United States

Mikhail A. Anisimov — Institute for Physical Science and Technology, University of Maryland, College Park, Maryland 20742, United States; Department of Chemical and Biomolecular Engineering, University of Maryland, College Park, Maryland 20742, United States; orcid.org/0000-0002-8598-949X

Complete contact information is available at: https://pubs.acs.org/10.1021/acs.jpcb.2c08901

#### Notes

The authors declare no competing financial interest.

#### ACKNOWLEDGMENTS

This work was inspired by the studies of the interfacial properties of polyamorphic liquids by Pablo Debenedetti and his co-workers. The authors thank Nikolay Shumovskyi for useful discussions on the Monte Carlo simulations of the blinking-checkers model. T.J.L. acknowledges the support of the Chateaubriand Fellowship of the Office for Science &

Technology of the Embassy of France in the United States. The research of T.J.L. and M.A.A. was partially supported by NSF Award No. 1856479. The research of S.V.B. was supported by NSF Award No. 1856496 and partially supported through the Bernard W. Gamson Computational Science Center at Yeshiva College. F.C. acknowledges the support of the Agence Nationale de la Recherche, Grant No. ANR-19-CE30-0035-01.

#### REFERENCES

- (1) Debenedetti, P. G. One substance, two liquids? *Nature* **1998**, 392, 127–128.
- (2) Stanley, H. E. In Advances in Chemical Physics; Stuart, A., Rice, A. R. D., Eds.; John Wiley & Sons: 2013; Vol. 152.
- (3) Anisimov, M. A.; Duška, M.; Caupin, F.; Amrhein, L. E.; Rosenbaum, A.; Sadus, R. J. Thermodynamics of Fluid Polyamorphism. *Phys. Rev. X* **2018**, *8*, 011004.
- (4) Tanaka, H. Liquid—liquid transition and polyamorphism. J. Chem. Phys. 2020, 153, 130901.
- (5) Vollhardt, D.; Wölfle, P. The Superfluid Phases of Helium 3; Taylor and Francis: London, 1990.
- (6) Schmitt, A. Introduction to Superfluidity. Lecture Notes in Physics; Springer International Publishing: Cham, Switzerland, 2015; Vol. 888
- (7) Ohta, K.; Ichimaru, K.; Einaga, M.; Kawaguchi, S.; Shimizu, K.; Matsuoka, T.; Hirao, N.; Ohishi, Y. Phase boundary of hot dense fluid hydrogen. *Sci. Rep.* **2015**, *5*, 16560.
- (8) Zaghoo, M.; Salamat, A.; Silvera, I. F. Evidence of a first-order phase transition to metallic hydrogen. *Phys. Rev. B* **2016**, 93, 155128.
- (9) McWilliams, R. S.; Dalton, D. A.; Mahmood, M. F.; Goncharov, A. F. Optical Properties of Fluid Hydrogen at the Transition to a Conducting State. *Phys. Rev. Lett.* **2016**, *116*, 255501.
- (10) Norman, G. E.; Saitov, I. M. Plasma Phase Transition. *Phys. Usp.* **2021**, *64*, 1094.
- (11) Fried, N. R.; Longo, T. J.; Anisimov, M. A. Thermodynamic modeling of fluid polyamorphism in hydrogen at extreme conditions. *J. Chem. Phys.* **2022**, *157*, 101101.
- (12) Henry, L.; Mezouar, M.; Garbarino, G.; Sifré, D.; Weck, G.; Datchi, F. Liquid—liquid transition and critical point in sulfur. *Nature* **2020**, *584*, 382—386.
- (13) Katayama, Y.; Mizutani, T.; Utsumi, W.; Shimomura, O.; Yamakata, M.; ichi Funakoshi, K. A first-order liquid—liquid phase transition in phosphorus. *Nature* **2000**, *403*, 170—173.
- (14) Katayama, Y.; Inamura, Y.; Mizutani, T.; Yamakata, M.; Utsumi, W.; Shimomura, O. Macroscopic Separation of Dense Fluid Phase and Liquid Phase of Phosphorus. *Science* **2004**, *306*, 848–851.
- (15) Glosli, J. N.; Ree, F. H. Liquid-Liquid Phase Transformation in Carbon. *Phys. Rev. Lett.* **1999**, *82*, 4659–4662.
- (16) Sastry, S.; Angell, C. A. Liquid-liquid phase transition in supercooled silicon. *Nat. Mater.* **2003**, *2*, 739–743.
- (17) Beye, M.; Sorgenfrei, F.; Schlotter, W. F.; Wurth, W.; Föhlisch, A. The liquid-liquid phase transition in silicon revealed by snapshots of valence electrons. *Proc. Natl. Acad. Sci. U. S. A.* **2010**, *107*, 16772–16776
- (18) Vasisht, V. V.; Saw, S.; Sastry, S. Liquid—liquid critical point in supercooled silicon. *Nat. Phys.* **2011**, *7*, 549–553.
- (19) Sciortino, F. Liquid-liquid transitions: Silicon in silico. *Nat. Phys.* **2011**, *7*, 523–524.
- (20) Saika-Voivod, I.; Sciortino, F.; Poole, P. H. Computer simulations of liquid silica: Equation of state and liquid—liquid phase transition. *Phys. Rev. E* **2000**, *63*, 011202.
- (21) Lascaris, E.; Hemmati, M.; Buldyrev, S. V.; Stanley, H. E.; Angell, C. A. Search for a liquid-liquid critical point in models of silica. *J. Chem. Phys.* **2014**, *140*, 224502.
- (22) Tsuchiya, Y.; Seymour, E. F. W. Thermodynamic properties of the selenium-tellurium system. *J. Phys. C Solid State Phys.* **1982**, *15*, L687–L695.

- (23) Brazhkin, V. V.; Popova, S. V.; Voloshin, R. N. Pressure -temperature phase diagram of molten elements: selenium, sulfur and iodine. *Physica B* **1999**, *265*, 64–71.
- (24) Cadien, A.; Hu, Q. Y.; Meng, Y.; Cheng, Y. Q.; Chen, M. W.; Shu, J. F.; Mao, H. K.; Sheng, H. W. First-Order Liquid-Liquid Phase Transition in Cerium. *Phys. Rev. Lett.* **2013**, *110*, 125503.
- (25) Angell, C. A. Two-State Thermodynamics and Transport Properties for Water as Zeroth-Order Results of a "Bond Lattice" Model. J. Phys. Chem. 1971, 75, 3698.
- (26) Angell, C. A. Amorphous Water. Annu. Rev. Phys. Chem. 2004, 55, 559-583.
- (27) Poole, P. H.; Sciortino, F.; Essmann, U.; Stanley, H. E. Phase Behavior of Metastable Water. *Nature* **1992**, *360*, 324–328.
- (28) Holten, V.; Anisimov, M. A. Entropy-driven liquid—liquid separation in supercooled water. Sci. Rep. 2012, 2, 713.
- (29) Holten, V.; Palmer, J. C.; Poole, P. H.; Debenedetti, P. G.; Anisimov, M. A. Two-state thermodynamics of the ST2 model for supercooled water. *J. Chem. Phys.* **2014**, *140*, 104502.
- (30) Gallo, P.; Amann-Winkel, K.; Angell, C. A.; Anisimov, M. A.; Caupin, F.; Chakravarty, C.; Lascaris, E.; Loerting, T.; Panagiotopoulos, A. Z.; Russo, J.; et al. Water: A Tale of Two Liquids. *Chem. Rev.* **2016**, *116*, 7463–7500.
- (31) Biddle, J. W.; Singh, R. S.; Sparano, E. M.; Ricci, F.; González, M. A.; Valeriani, C.; Abascal, J. L. F.; Debenedetti, P. G.; Anisimov, M. A.; Caupin, F. Two-structure thermodynamics for the TIP4P/2005 model of water covering supercooled and deeply stretched regions. *J. Chem. Phys.* **2017**, *146*, 034502.
- (32) Caupin, F.; Anisimov, M. A. Thermodynamics of supercooled and stretched water: Unifying two-structure description and liquid-vapor spinodal. *J. Chem. Phys.* **2019**, *151*, 034503.
- (33) Duška, M. Water above the spinodal. J. Chem. Phys. **2020**, 152, 174501.
- (34) Holten, V.; Qiu, C.; Guillerm, E.; Wilke, M.; Rička, J.; Frenz, M.; Caupin, F. Compressibility Anomalies in Stretched Water and Their Interplay with Density Anomalies. *J. Phys. Chem. Lett.* **2017**, *8*, 5519–5522
- (35) Kim, K. H.; Späh, A.; Pathak, H.; Perakis, F.; Mariedahl, D.; Amann-Winkel, K.; Sellberg, J. A.; Lee, J. H.; Kim, S.; Park, J.; et al. Maxima in the thermodynamic response and correlation functions of deeply supercooled water. *Science* **2017**, 358, 1589–1593.
- (36) Pathak, H.; Späh, A.; Esmaeildoost, N.; Sellberg, J. A.; Kim, K. H.; Perakis, F.; Amann-Winkel, K.; Ladd-Parada, M.; Koliyadu, J.; Lane, T. J.; et al. Enhancement and maximum in the isobaric specificheat capacity measurements of deeply supercooled water using ultrafast calorimetry. *Proc. Natl. Acad. Sci. U. S. A.* **2021**, *118*, No. e2018379118.
- (37) Hacker, P. T. Experimental values of the surface tension of supercooled water. NASA Tech. Note 1951, 2510, 1.
- (38) Floriano, M. A.; Angell, C. A. Surface tension and molar surface free energy and entropy of water to -27.2 degree C. *J. Phys. Chem.* **1990**, *94*, 4199–4202.
- (39) Trinh, E. H.; Ohsaka, K. Measurement of density, sound velocity, surface tension, and viscosity of freely suspended supercooled liquids. *Int. J. Thermophys* **1995**, *16*, 545–555.
- (40) Hrubý, J.; Vins, V.; Mares, R.; Hykl, J.; Kalova, J. Surface Tension of Supercooled Water: No Inflection Point down to 25 °C. *J. Phys. Chem. Lett.* **2014**, *5*, 425–428.
- (41) Vinš, V.; Fransen, M.; Hykl, J.; Hrubý, J. Surface Tension of Supercooled Water Determined by Using a Counterpressure Capillary Rise Method. *J. Phys. Chem. B* **2015**, *119*, 5567–5575.
- (42) Vinš, V.; Hošek, J.; Hykl, J.; Hrubý, J. Surface Tension of Supercooled Water: Inflection Point-Free Course down to 250 K Confirmed Using a Horizontal Capillary Tube. *J. Chem. Eng. Data* **2017**, *62*, 3823–3832.
- (43) Vinš, V.; Hykl, J.; Hrubý, J.; Blahut, A.; Celný, D.; Čenský, M.; Prokopová, O. Possible Anomaly in the Surface Tension of Supercooled Water: New Experiments at Extreme Supercooling down to -31.4 degree C. J. Phys. Chem. Lett. 2020, 11, 4443-4447.

- (44) Feeney, M. R.; Debenedetti, P. G. A Theoretical Study of the Interfacial Properties of Supercooled Water. *Ind. Eng. Chem. Res.* **2003**, *42*, 6396–6405.
- (45) Hrubý, J.; Holten, V. A two-structure model of thermodynamic properties and surface tension of supercooled water. *Proceedings of the 14th International Conference on the Properties of Water and Steam, Maruzen.* 2004, 241–246.
- (46) Lü, Y. J.; Wei, B. Second inflection point of water surface tension. *Appl. Phys. Lett.* **2006**, *89*, 164106.
- (47) Wang, X.; Binder, K.; Chen, C.; Koop, T.; Pöschl, U.; Su, H.; Cheng, Y. Second inflection point of water surface tension in the deeply supercooled regime revealed by entropy anomaly and surface structure using molecular dynamics simulations. *Phys. Chem. Chem. Phys.* **2019**, *21*, 3360–3369.
- (48) Rogers, T. R.; Leong, K.-Y.; Wang, F. Possible Evidence for a New Form of Liquid Buried in the Surface Tension of Supercooled Water. *Sci. Rep.* **2016**, *6*, 33284.
- (49) Malek, S. M. A.; Poole, P. H.; Saika-Voivod, I. Surface tension of supercooled water nanodroplets from computer simulations. *J. Chem. Phys.* **2019**, *150*, 234507.
- (50) Gorfer, A.; Dellago, C.; Sega, M. High-density liquid (HDL) adsorption at the supercooled water/vapor interface and its possible relation to the second surface tension inflection point. *J. Chem. Phys.* **2023**, *158*, 054503.
- (51) Singh, R. S.; Palmer, J. C.; Panagiotopoulos, A. Z.; Debenedetti, P. G. Thermodynamic analysis of the stability of planar interfaces between coexisting phases and its application to supercooled water. *J. Chem. Phys.* **2019**, *150*, 224503.
- (52) Caupin, F.; Anisimov, M. A. Minimal Microscopic Model for Liquid Polyamorphism and Waterlike Anomalies. *Phys. Rev. Lett.* **2021**, 127, 185701.
- (53) Ciach, A.; Góźdź, W.; Perera, A. Simple three-state lattice model for liquid water. *Phys. Rev. E* **2008**, 78, 021203.
- (54) Sastry, S.; Debenedetti, P. G.; Sciortino, F.; Stanley, H. E. Singularity-free interpretation of the thermodynamics of supercooled water. *Phys. Rev. E* **1996**, *53*, 6144–6154.
- (55) Stokely, K.; Mazza, M. G.; Stanley, H. E.; Franzese, G. Effect of hydrogen bond cooperativity on the behavior of water. *Proc. Natl. Acad. Sci. U. S. A.* **2010**, *107*, 1301–1306.
- (56) Cerdeiriña, C. A.; Troncoso, J.; González-Salgado, D.; Debenedetti, P. G.; Stanley, H. E. Water's two-critical-point scenario in the Ising paradigm. *J. Chem. Phys.* **2019**, *150*, 244509.
- (57) Harvey, A. H.; Hrubý, J.; Meier, K. Improved and Always Improving: Reference Formulations for Thermophysical Properties of Water. J. Phys. Chem. Ref. Data 2023, 52, 011501.
- (58) Landau, L. D.; Lifshitz, E. M. Statistical Physics: Part 2, 2nd ed.; Pergamon Press: Oxford, U.K., 1981; Vol. 9.
- (59) Fisher, M. E. In *Critical Phenomena*; Hahne, F. J. W., Ed.; Lecture Notes in Physics; Springer: Berlin, Heidelberg, 1983; pp 1–139.
- (60) Leung, S. S.; Griffiths, R. B. Thermodynamic Properties near the Liquid-Vapor Critical Line in Mixtures of He<sup>3</sup> and He<sup>4</sup>. *Phys. Rev.* A **1973**, *8*, 2670–2683.
- (61) Jin, G.; Tang, S.; Sengers, J. Thermodynamic behavior of fluid mixtures in the critical region. Fluid Phase Equilib. 1992, 75, 1–10.
- (62) Anisimov, M.; Sengers, J. On the choice of a hidden field variable near the critical point of fluid mixtures. *Phys. Lett. A* **1992**, 172, 114–118.
- (63) Debye, P. Angular Dissymmetry of the Critical Opalescence in Liquid Mixtures. *J. Chem. Phys.* **1959**, *31*, 680.
- (64) Yang, A. J. M.; Fleming, P. D.; Gibbs, J. H. Molecular theory of surface tension. *J. Chem. Phys.* **1976**, *64*, 3732.
- (65) Lu, B. Q.; Evans, R.; da Gama, M. T. The form of the density profile at a liquid-gas interface. *Mol. Phys.* 1985, 55, 1319–1338.
- (66) Kahl, H.; Enders, S. Interfacial properties of binary mixtures. *Phys. Chem. Chem. Phys.* **2002**, *4*, 931–936.
- (67) Stephan, S.; Hasse, H. Molecular interactions at vapor-liquid interfaces: Binary mixtures of simple fluids. *Phys. Rev. E* **2020**, *101*, 012802.

- (68) van der Waals, J. D. Thermodynamische Theorie de Capillariteit in de Onderstelling van Coninue Dichtheidsverandering. Verhand. Konink. Akad. Wetensch. Amsterdam. (Sect. 1) 1893, 1, 56.
- (69) Rowlinson, J. S.; Widom, B. Molecular Theory of Capillarity; Oxford University Press: Oxford, U.K., 1982.
- (70) Cahn, J. W.; Hilliard, J. E. Free Energy of a Nonuniform System. I. Interfacial Free Energy. J. Chem. Phys. 1958, 28, 258.
- (71) Poser, C. I.; Sanchez, I. C. Surface tension theory of pure liquids and polymer melts. J. Colloid Interface Sci. 1979, 69, 539-548.
- (72) Poser, C. I.; Sanchez, I. C. Interfacial Tension Theory of Low and High Molecular Weight Liquid Mixtures. Macromol. 1981, 14, 361 - 370.
- (73) Fisher, M. P. A.; Wortis, M. Curvature corrections to the surface tension of fluid drops: Landau theory and a scaling hypothesis. Phys. Rev. B 1984, 29, 6252-6260.
- (74) Anisimov, M. A.; Bertrand, C. E. In Applied Thermodynamics of Fluids; Goodwin, A. R., Peters, C. J., Sengers, J., Eds.; Royal Society of Chemistry: Cambridge, U.K., 2010; Chapter 7, pp 172-214.
- (75) Singh, Y.; Santra, M.; Singh, R. S. Anomalous Vapor and Ice Nucleation in Water at Negative Pressures: A Classical Density Functional Theory Study. ArXiv 2022, 2212.07147.
- (76) Caupin, F. Liquid-vapor interface, cavitation, and the phase diagram of water. Phys. Rev. E 2005, 71, 051605.
- (77) Anisimov, M.; Gorodetskii, E.; Kulikov, V.; Povodyrev, A.; Sengers, J. A general isomorphism approach to thermodynamic and transport properties of binary fluid mixtures near critical points. Physica A 1995, 220, 277-324.
- (78) Anisimov, M. A.; Wang, J. Nature of Asymmetry in Fluid Criticality. Phys. Rev. Lett. 2006, 97, 025703.
- (79) Wang, J.; Anisimov, M. A. Nature of vapor-liquid asymmetry in fluid criticality. Phys. Rev. E 2007, 75, 051107.
- (80) Bertrand, C. E.; Anisimov, M. A. Complete Scaling for Inhomogeneous Fluids. Phys. Rev. Lett. 2010, 104, 205702.
- (81) Abascal, J. L. F.; Vega, C. Widom line and the liquid-liquid critical point for the TIP4P/2005 water model. J. Chem. Phys. 2010, 133, 234502.
- (82) Debenedetti, P. G.; Sciortino, F.; Zerze, G. H. Second critical point in two realistic models of water. Science 2020, 369, 289-292.

# **□** Recommended by ACS

Persistent Local Structural Defectiveness as an Early Time **Predictor of Intermittent Glassy Relaxation Events in Supercooled Water** 

Alejandro R. Verde, Gustavo A. Appignanesi, et al.

APRIL 06, 2023

THE IOURNAL OF PHYSICAL CHEMISTRY B

**Characterization of the Pure Black Tea Wine Fermentation Process by Electronic Nose and Tongue-Based Techniques** with Nutritional Characteristics

Jing Chen, Gan-Lin Chen, et al.

MARCH 22 2023

ACS OMEGA

READ **C** 

Methane Storage by Forming sII Hydrate in the Presence of a Novel Kinetic Promoter with the Function of Alleviating the **Wall-Climbing Growth** 

Liang Mu, Qingyan Cui, et al.

MARCH 16, 2023

**ENERGY & FUELS** 

RFAD 17

#### Glass Polymorphism in Hyperquenched Aqueous LiCl **Solutions**

Johannes Giebelmann, Thomas Loerting, et al.

APRIL 07, 2023

THE JOURNAL OF PHYSICAL CHEMISTRY B

RFAD 🗹

Get More Suggestions >